

FINAL  
IN-35-CR  
ICIT  
3 REF  
65070  
p-29

---

# FINAL REPORT

(May 1st. 1995)

## DEVELOPMENT OF A FIBER OPTIC COMPRESSOR BLADE SENSOR

(NASA Grant Contract NAG3186)  
(SUNY Grant Number 431 4890A)  
Grant Monitor: Dr. Anatole Kurkov, MS23-1

Award Period: 09/08/93 to 09/07/94

### Principal Investigator

Harbans Singh Dhadwal  
Associate Professor  
State University of New York  
Department of Electrical Engineering  
Stony Brook, NY 11794-2350

Tel: (516) 632 8396  
Fax: (516) 632 8494  
email: dhadwal@sbee.sunysb.edu

---

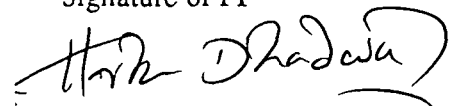
(NASA-CR-199298) DEVELOPMENT OF A  
FIBER OPTIC COMPRESSOR BLADE SENSOR  
Final Report, 8 Sep. 1993 - 7 Sep.  
1994 (State Univ. of New York)  
29 p

N96-15993

Unclas

G3/35 0065070

Submitted on May 1st, 1995  
Signature of PI



---

## CONTENTS

Executive Summary .....	i
Acknowledgements .....	ii
Dissemination of Research Results .....	ii
1 Introduction .....	1
2 Theoretical Background .....	2
3 Experimental Results .....	5
3.1 Signal Detection Processing and Data Acquisition .....	6
3.2 Tip Clearance Results .....	7
3.3 Dynamic Testing .....	9
4 Discussion .....	16
5 References .....	17
6 Appendices .....	18

---

---

## EXECUTIVE SUMMARY

All the goals of the original proposal were realized. A complete working prototype of the fiber optic blade tip sensor was first tested in the laboratory, followed by a thorough evaluation at NASA W8 Single Compressor Stage Facility in Lewis Research Center. Subsequently, a complete system with three parallel channels was fabricated and delivered to Dr. Kurkov. The final system was tested in the Subsonic Wind Tunnel Facility, in parallel with The General Electric Company's light probe system. The results at all operating speeds were comparable. This report provides a brief description of the system and presents a summary of the experimental results.

---

## ACKNOWLEDGEMENTS

I want to thank the Chief of the Structural Dynamics Division at the NASA Lewis Research Center for the financial support for this project. I have enjoyed the participation and encouragement of Dr. Anatole Kurkov throughout the project and want to express my sincere appreciation for his assistance. I wish to acknowledge the professionalism and assistance of the staff operating the single compressor stage and the 9X15 subsonic wind tunnel facilities at LeRc; their patience and cooperation made the testing of the hardware an enjoyable experience. I also want to thank Dr. Paul Mosey and the General Electric Company for allowing us access to their experimental engine and for staying an extra two days on our account. I also wish to thank Dr. Oral Mehmed for many useful discussions at the Lewis Research Center.

## DISSEMINATION OF RESEARCH RESULTS

1. Ali Mehmed, "Fiber Optic Sensor For Measurement of Deflection and Tip Clearance in Compressor Blades," M.Sc. Thesis, State University of New York, December 1994 (A copy of the thesis was submitted to Dr. Kurkov in January 1995).
2. Harbans S. Dhadwal, Ali Mehmed, Anatole Kurkov, and Romel R. Khan, "A Fiber Optic System For Deflection Measurements," manuscript in preparation
3. An Invention Disclosure, "A Fiber Optic System Deflection and Displacement of compressor," was filed with the State University of New York on August 17, 1994.

## 1. INTRODUCTION

Accurate measurements of the blade tip dynamics in the compressor stage are essential for the design of high performance engines. These measurements provide designers with vital information which can be used to assess the accuracy of a particular mathematical model. Modelling of the dynamic behavior of the blade tip requires precise knowledge of each blade tip under various operating speeds. The leading and trailing edge of each blade can be located relative to the one per revolution signal; this is achieved through optical scanning of the blade tip. The sensitivity of the measurement is specified in terms of the rise and fall time of the scanning system.

This final report describes the design and testing of a fiber optic system for real time monitoring of blade tip dynamics. A means of measuring the timing information of the leading and trailing edge of the blade tip and real time monitoring of the blade tip clearance. Figure 1 shows a photograph of the complete system, which comprises a set of fiber optic sensor heads, and an electronics module, containing the laser transmitters and receivers. Design of each subassembly is described below. The system provides a 100 ns timing resolution for each of the channels. The system is modular in design allowing for easy expansion to any number of timing channels.

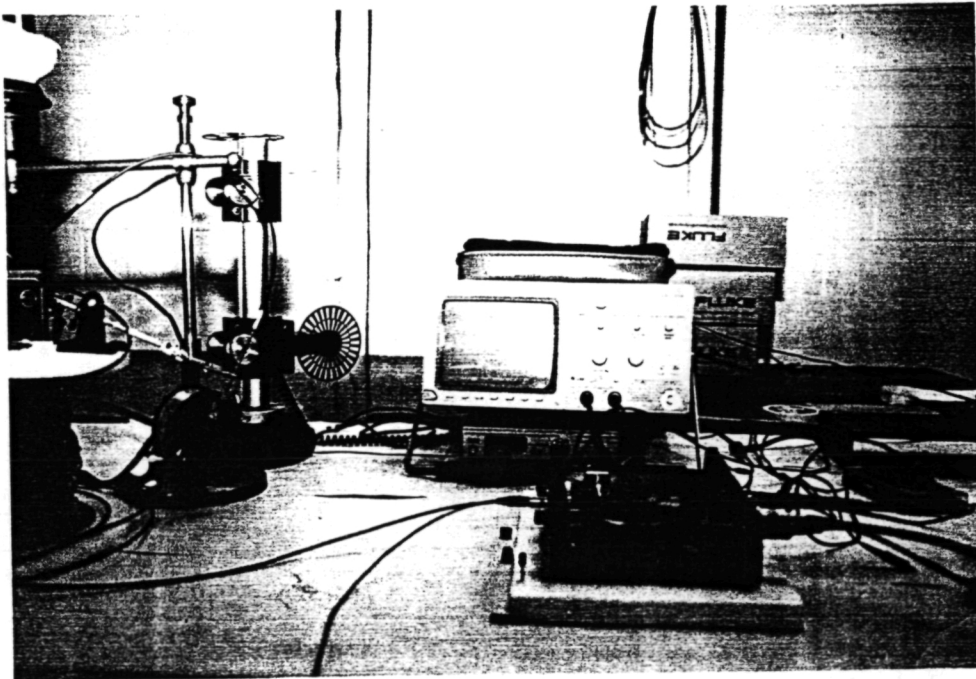


Figure 1: Fiber optic system for measuring blade tip dynamics

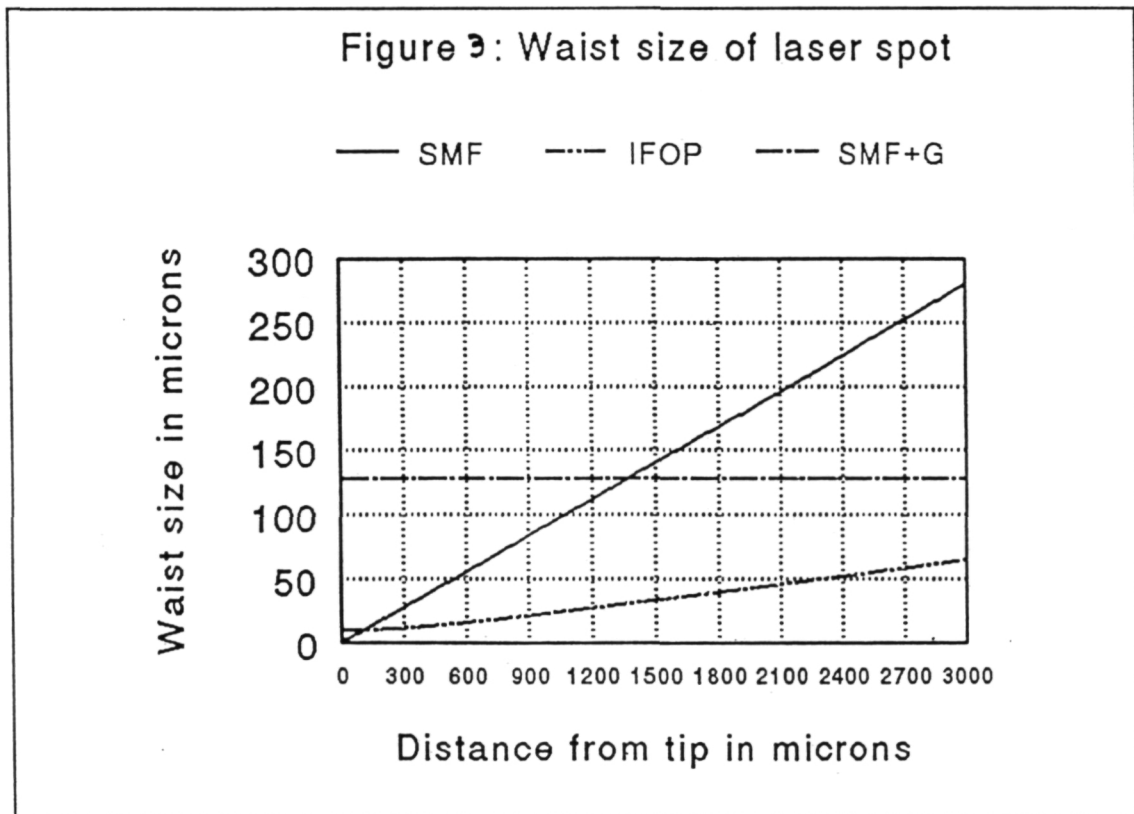
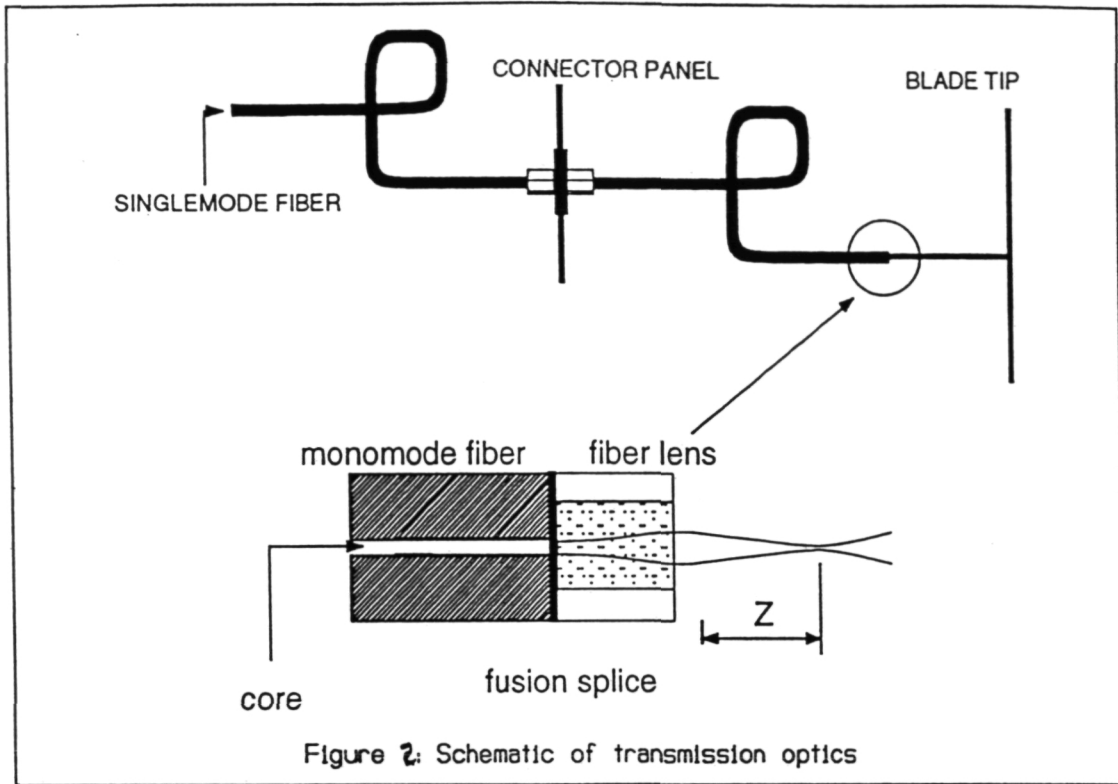
## 2. THEORETICAL BACKGROUND

Present day sensors for vibration monitoring and measurements are based on non-invasive optical techniques<sup>1-3</sup>. Typically, a fiber optic probe, comprising transmitting and receiving optics in a single cylindrical housing, is precisely positioned into the engine casing. Circumferential positioning of several probes, together with the data acquisition and processing, permits measurements of both blade vibration and steady state blade deflection. These optical sensors combine fiber optics and gradient index (GRIN) microlens technologies to achieve the necessary miniaturization and efficiency. Semiconductor laser sources and detectors are routinely integrated into the system. In this manner, small spatially coherent spots of light can be delivered remotely to a target, and the diffused light scattered in the backward direction can be collected efficiently.

In this project, the latest technology of integrated fiber optics (IFO)<sup>4</sup>, developed at Stony Brook, was utilized in the design of fiber optic sensors for monitoring blade deflections. IFO, through wavefront engineering, permits sufficient control for the delivery of focussed or collimated optical energy to a remote target. Wavefront control of optical wavefields propagating inside monomode optical fibers is achieved through selection of appropriate refractive index profile and length of a graded index multimode optical fiber, which is fusion spliced to a monomode optical fiber.

IFO reduces fabrication complexity by eliminating the mis-match between the size of GRIN microlenses and monomode optical fibers. Subsequently, the diameter of a transmitting probe is reduced from 2 mm to 0.125 mm. A fiber optic blade tip sensor described below utilizes IFO to deliver a 50  $\mu\text{m}$  spatially coherent light spot to a blade tip located at a distance of 2.5 mm from the probe tip. A ring of multimode optical fibers can collect more than 2% of the total optical power radiated into the hemisphere normal to the blade tip.

Figure 2 shows a schematic of an integrated fiber optic based laser delivery system. A short length of a multimode gradient index optical fiber is fusion spliced to a singlemode optical fiber transmitting laser power from the transmitter module located in the control room to the wind tunnel section. The final timing specification of the complete system is determined by the size of the scanning optical spot as well as the bandwidth of the electronic receiver module. The smaller the spot size the faster the rise time of the optical receiver. Essentially the apparent width of the blade is proportional to the diameter of the scanning laser spot; a small scanning laser spot permits timing information to be derived from thin blade sections, typically, less than 0.002". Conventional means of laser delivery to the blade tip are impractical, a system using a gradient index cylindrical lens is possible, but as shown in Fig 3, is also not useful. The integrated approach eliminates alignment problems, while adequately meeting the stringent spatial requirements, that is, an outer diameter of the probe which is less than 0.1".



The blade tip is assumed to be a Lambertian source with sterance  $L_T$  [ $\text{W}\cdot\text{m}^{-2}\text{Sr}^{-1}$ ], which is related to the illuminating incidence  $E_T$  [ $\text{W}\cdot\text{m}^{-2}$ ] through the relation

$$L_T = \frac{1}{\pi} E_T R_T$$

where  $R_T$  is the blade reflectance. As shown in Fig.4, an array of multimode optical fibers are arranged in a circular ring surrounding the transmitting probe. Using geometric arguments the optical power  $P_{FR}$ , received by the fiber array, can be expressed as a fraction of the total optical power  $P_T$  radiated into the hemisphere above the blade tip, that is,

$$\frac{P_{FR}}{P_T} = \pi \frac{a^2}{z^2} 2k \left[ 1 + \left( \frac{2kb}{z} \right)^2 \right]^{\frac{5}{2}} \quad k = 1, 2, 3$$

where  $a$  and  $b$  are the radii of the core and cladding, respectively, of a single receiving optical fiber,  $z$  is the distance from the blade tip to the receiving fiber ring, and  $k$  is an integer defining the ring order.

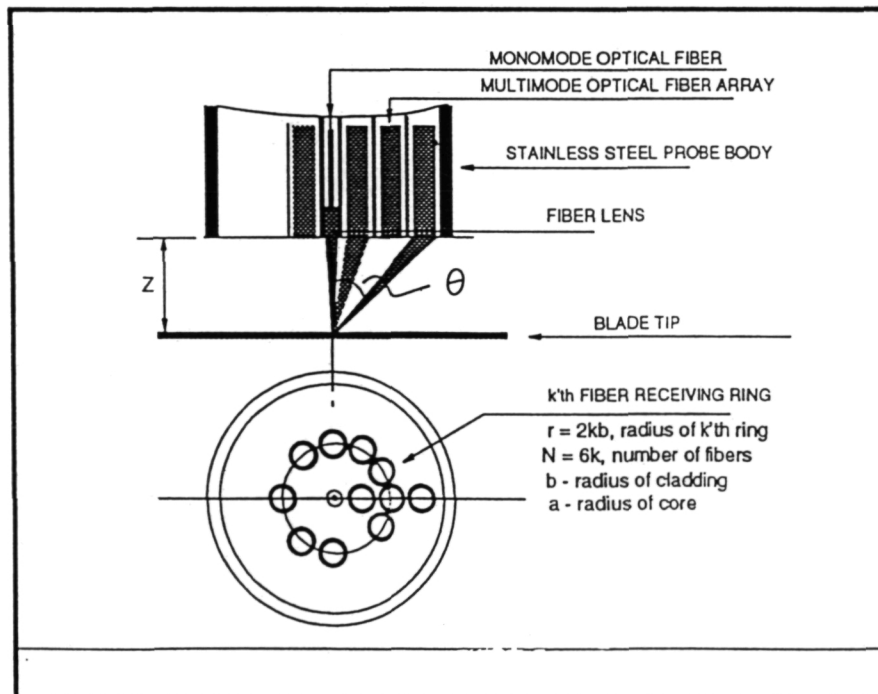


Figure 4: A schematic of the blade tip sensor

### 3. EXPERIMENTAL RESULTS

The physical arrangement of the probe is shown in Fig 5. Laser light is transported through the probe and focused into a spot on the turbine blade tip; the spot diameter is  $100\mu\text{m}$  at a distance of  $2\text{mm}$ . The diffusely scattered light from the blade surface is collected by an array of high numerical aperture optical fibers. The optical signal is then guided to the APD receiver. The probe can be considered in two sections, the transmitting and receiving section. The fiber probes were fabricated with six multimode fibers as shown in Fig 5; it was difficult to arrange the receiving fiber in an annular ring surrounding the transmitting fiber.

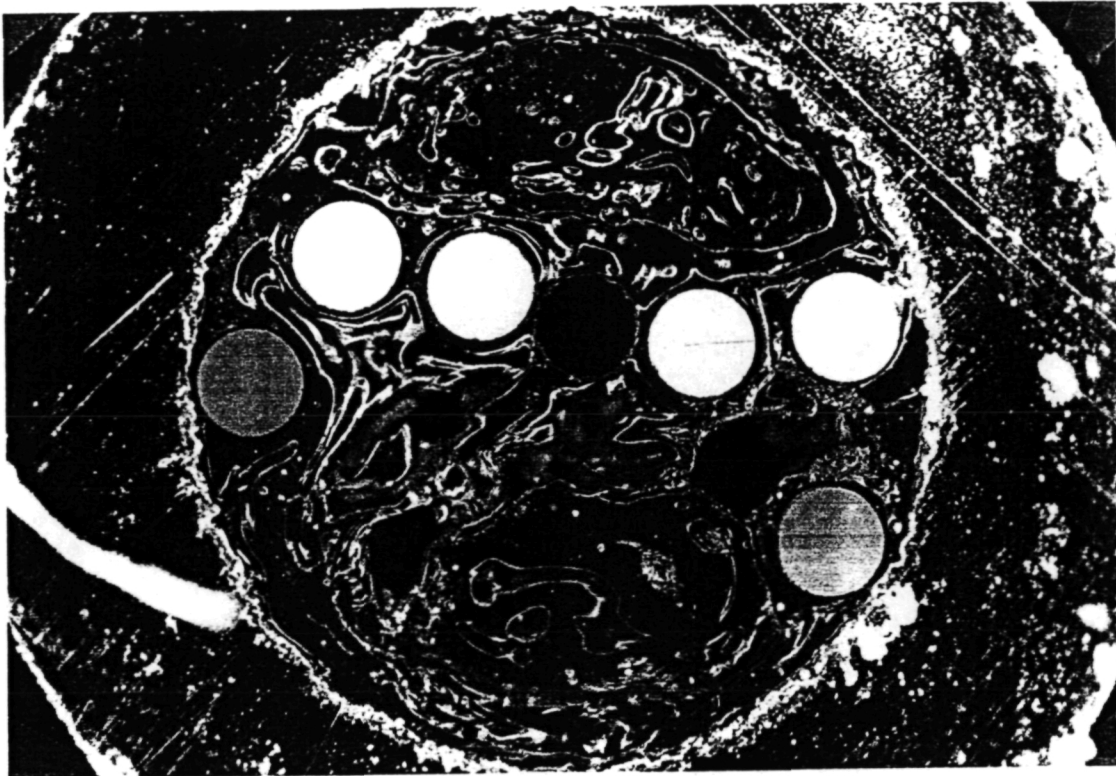


Figure 5 Photomicrograph of the probe face (magnification 100X, yellow fibers are receiving fibers, and the red spot is the core of the transmitting fiber)

The transmitting section consists of a  $4/125\mu\text{m}$  single mode optical fiber which emits approximately  $2.2\text{mW}$  of optical power at a wavelength of  $675\text{nm}$  out of the probe, (the bright red spots hitting the blade surface in Fig 5). The optical wavefront of the laser light emanating from the single mode fiber is processed, in-line, by fusion splicing a short section ( $\approx 300\mu\text{m}$ ) of gradient index multimode fiber  $50/125\mu\text{m}$ . The diverging spherical wavefront is transformed to a converging wavefront, with the image point at a distance of  $2\text{mm}$  from the fiber tip. The optical probes,  $0.094''$  in diameter, were mounted from the side of the engine through specially designed holes.

### 3.1 Signal Detection Processing and Data Acquisition

The diffused scattered light from the blade tip is collected by six high numerical aperture multimode optical fibers arranged in an array on both sides of the transmitting fiber. The fibers are cabled in a loose 3mm monocoil tubing which is about 150 feet long. The sensing end of the fiber cable is terminated in a stainless steel tubing of 0.094" diameter. At the other end of the fiber cable the transmitting fiber is terminated with a FC/PC connector and the six multimode fibers are mounted in a stainless steel ferrule and inserted into a second stainless steel tubing containing a Selfoc microlens. The FC/PC connector permits easy alignment free coupling, to a semiconductor laser.

The gain adjusting maintains electronic signals within the linear operation limits of the analog processing elements. With these design constraints the circuitry was operated with a bandwidth of 2 MHz, a higher bandwidth is also possible. Figure 6 shows a schematic of the receiver circuitry.

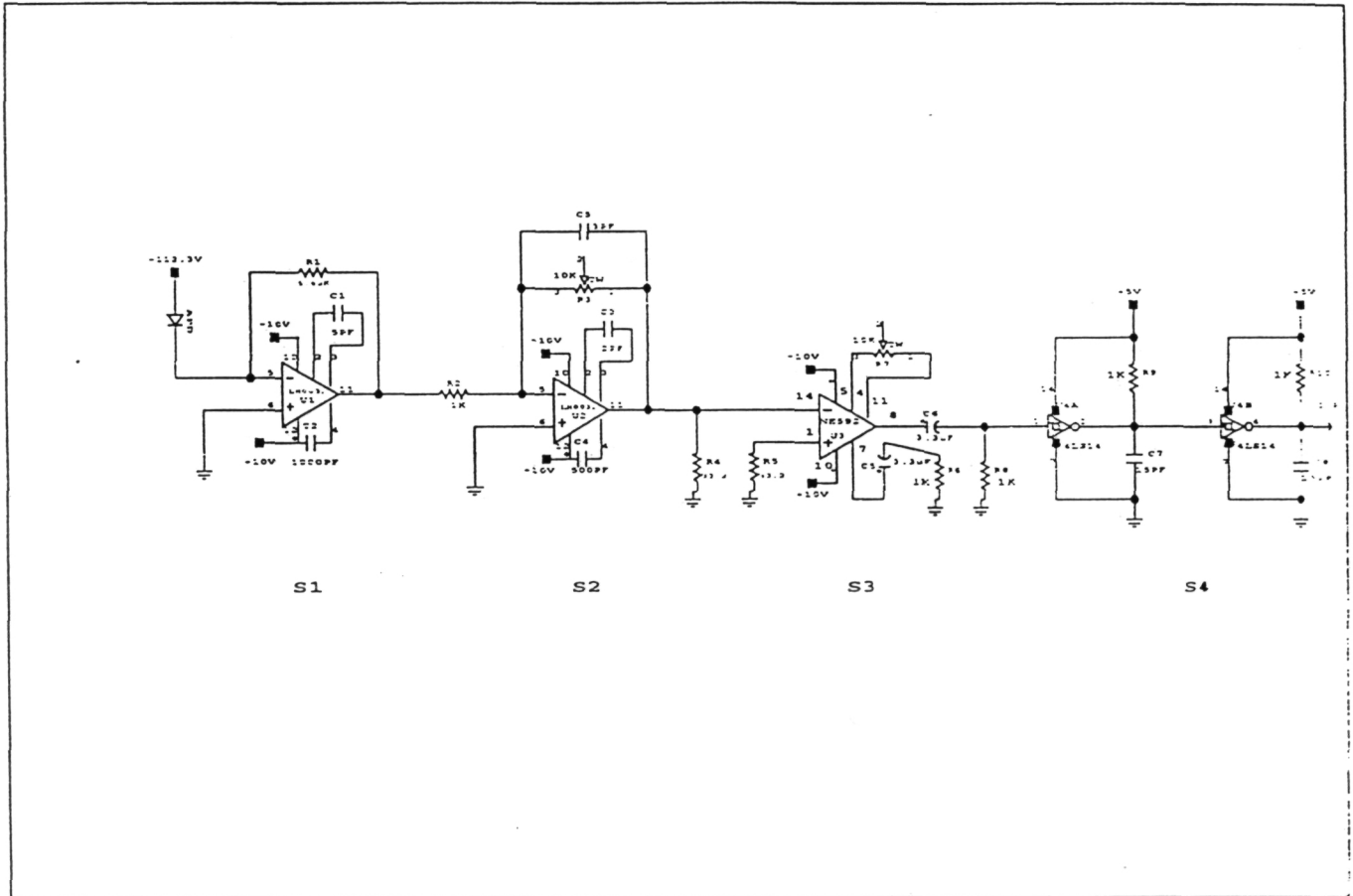


Figure6: A schematic of the receiver.

### 3.2 Tip Clearance Results

A static calibration was performed with the optical probe mounted in a micrometer calibration fixture as shown in Fig 7; this curve shows that a linear range is obtainable over approximately 0.025 inches with a resolution of 50 V/inch (0.00002 inch per mV).

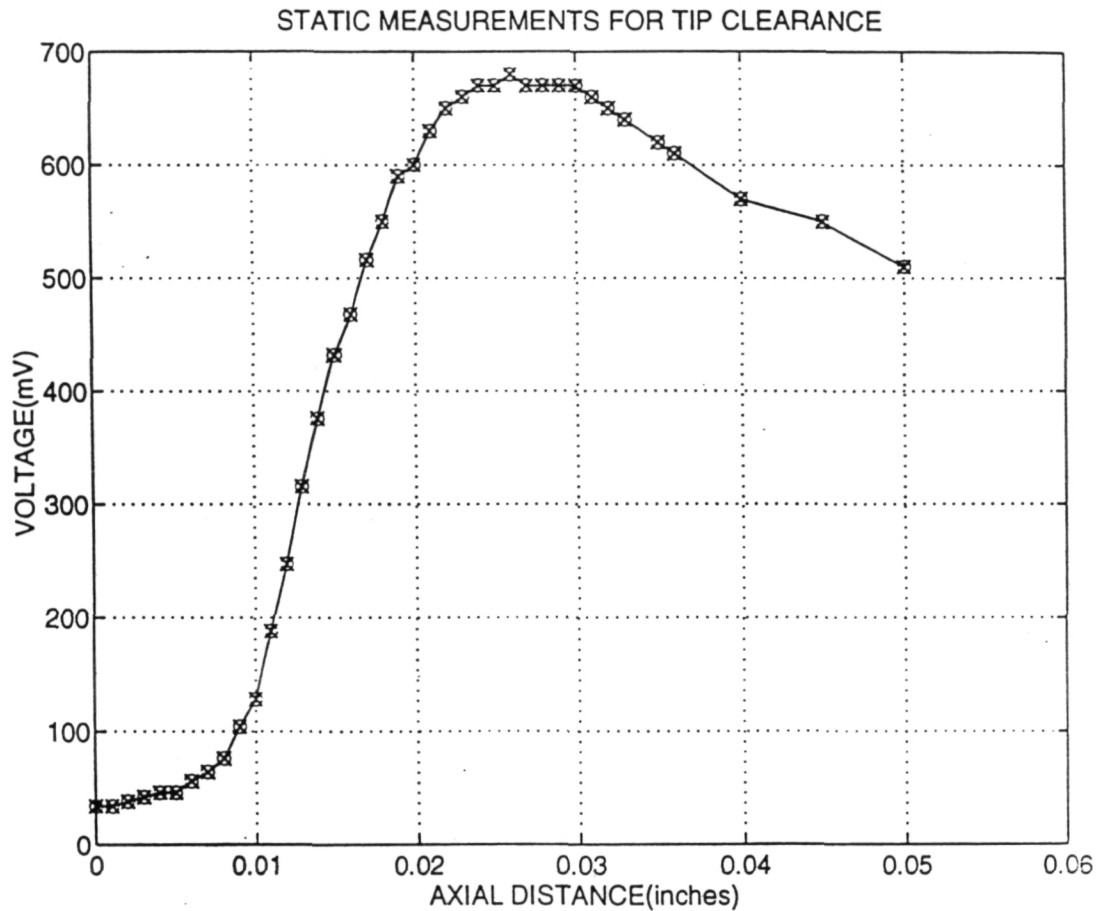


Figure 7: Static calibration curve for tip clearance measurements.

Dynamic tip clearance measurements were performed in the subsonic wind tunnel. The signals were recorded from the video stage just before the wave shaping stage of the sensor, in order to obtain the true shape of the pulses. For this reason each pulse is averaged over three revolutions in order to determine the exact voltage level at the corresponding speed. Figure 8 shows a typical voltage waveform obtained from one of the blade tips; it clearly shows the need for averaging in order to obtain a meaningful interpretation of the tip clearance. A blade tip rotating at 10,000 rpm requires 18 ms for this measurement. Figure 9 shows the variation of the average pulse height (mV) between the different blades, at two different speeds. From the above calibration it should be recalled that a change of 1 mV corresponds to a movement in the blade tip of 0.00002 inch.

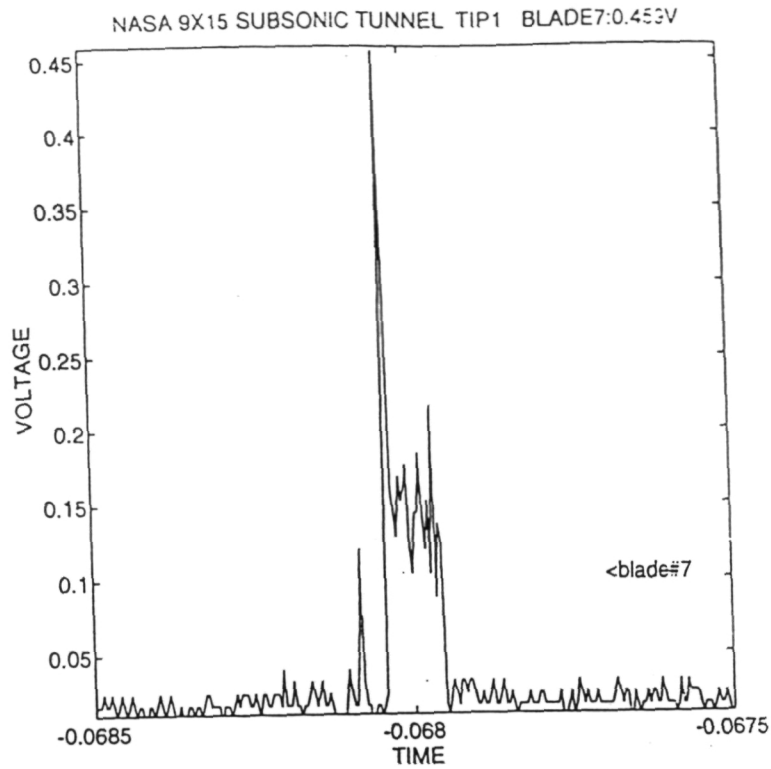


Figure 8: A typical voltage wave form obtained from blade #1 at a speed of 7% rpm

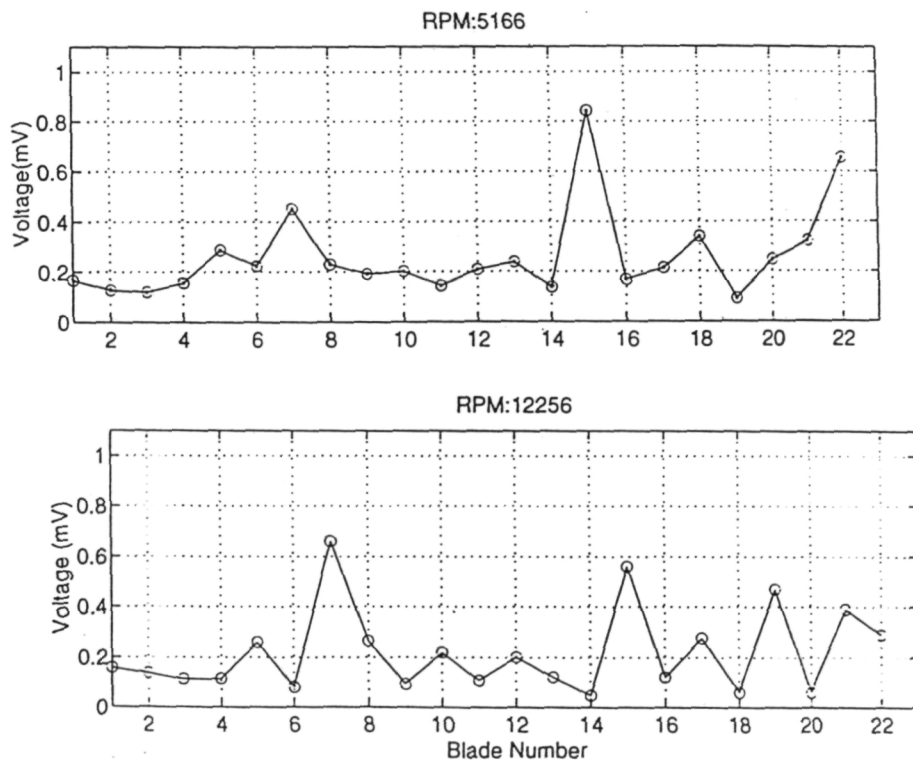


Figure 9: Variation of blade tip clearance for different blades at two speeds: (a) 40%, (b) 95% rpm

### 3.3 Dynamic Testing

A dynamic testing for evaluating the performances of the optical blade tip and vibration measurement system was done in a Single Stage Transonic Compressor facility and in a subsonic wind tunnel having a test section of 9 x 15 ft at NASA, Lewis Research Center.

#### 3.3.1 Single Stage Transonic Compressor Facility:

The transonic compressor shown in Fig 10 has a 20" diameter blade cluster which has 32 blades on it. A maximum mass flow rate of 70 lbm/s is achieved through 3000 hp drive motor with a maximum RPM of 20,000. Each blade has a tip (midchord) thickness of 0.15 inch. The casing of the compressor outside of the test wheel is modified to accept the optical probe, which is centered over the mid chord section of the blade and can be used to measure the static deflection in the individual blade. Figure 11 shows a typical pulse shape at 95% rpm for blade #1.

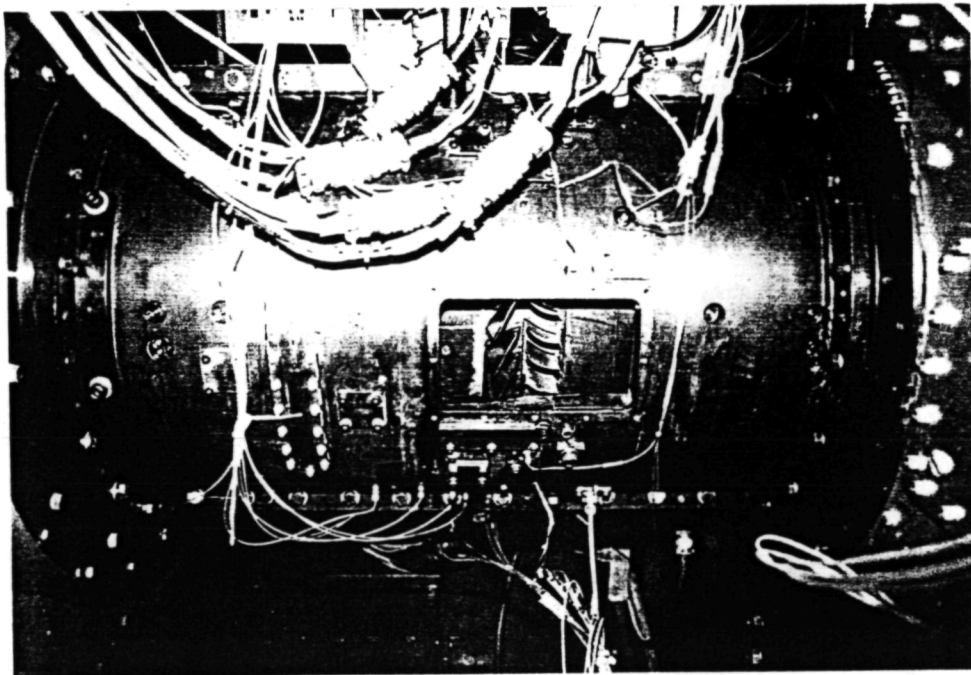


Figure 10: Photograph of the single stage compressor

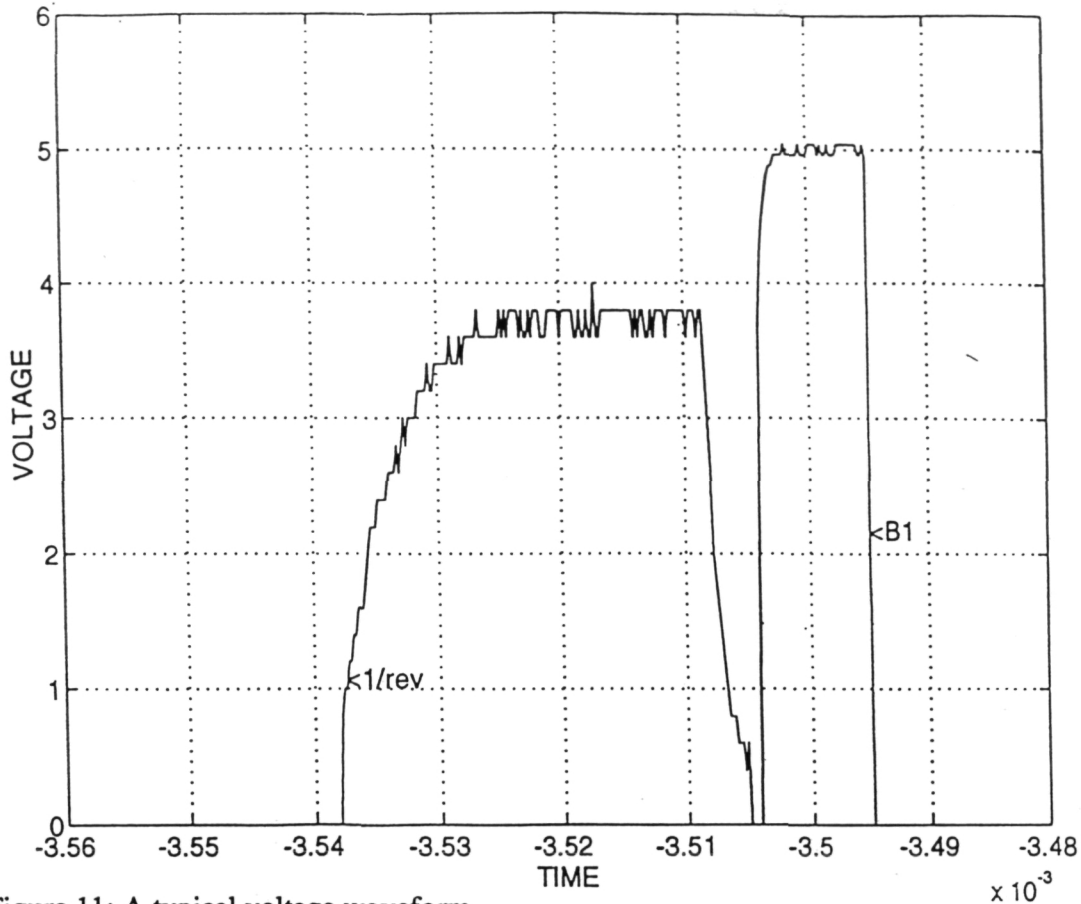


Figure 11: A typical voltage waveform

### 3.3.2 Subsonic Wind Tunnel Test Results

This test was performed on a General Electric engine, which had 22 composite blades, tip-to-tip diameter of 22 inches, the maximum RPM was 14,500 with a tip speed of 1180 ft/sec. A section of the wind tunnel with the engine mounted inside is shown in Fig. 12. The casing of the engine is modified to accept six optical probes as previously shown in Fig. 12; the probes are positioned along the blade chord. The laser supply and detection system were in the control room at a distance of 120 ft. Optical signals from the sensors were acquired through the 120 feet long fiber optic cables. Data was stored on the computer and the signals were displayed on a scope

Figure 13 shows a typical individual voltage traced as a function of time as a single blade passes the sensor. The signal clearly rises very sharply as the blade comes into view. This feature is to be expected of the optical probe since the probe has no knowledge of an approaching blade until the blade comes in its field of view. Probes based on capacitance or eddy current will have some awareness of an approaching blade as the fields for these sensors are not restricted to a direct line of sight. A signal appears transient just after the blade has come into view due to partial spot forming on the leading edge of the blade. The minor signal variations appearing in the central portion of the blade passage would appear to reflect small repeatable features of each blade. The electronics is set to gate the signal and to avoid picking up initial edge transient.



Figure 14 shows the digital pulse of the leading edge and the trailing edge of the blade, respectively. In order to determine the flutter in the blades, the digital pulses from the blade under observation at different rpms are superimposed in order to see the shift in the blade pulses. The shift can be translated into degrees in order to determine the blade deflection.

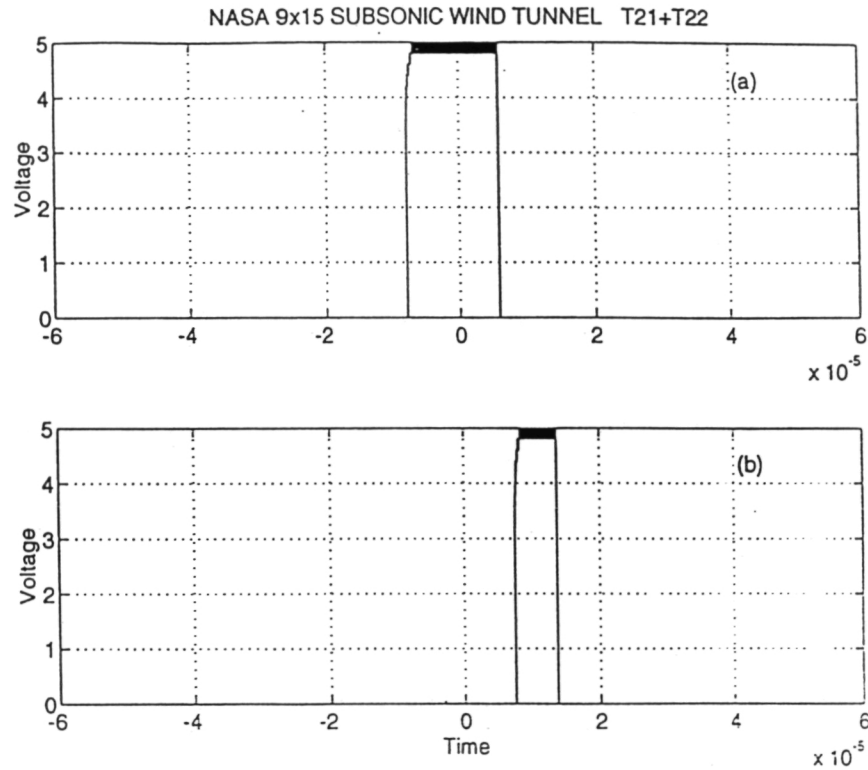


Figure 14: Digital pulse obtained from the (a) leading, and (b) trailing edges of the blade tip.

For tangential deflection analysis the first blade is defined as the blade that follows the positive edge of the 1/rev pulse plus the delay that is equivalent to five degrees of rotation counting from the positive edge of 1/rev. The blades are then counted as they pass the sensors. Units are in degrees for tangential direction. Figures 16,17 and 18 shows the tangential deflection at leading edge, midchord and trailing edge of the blades, respectively, at different RPMs; only the leading edges are plotted in the figures.

Figure 16: Plot of tangential deflection vs. blade at leading edge

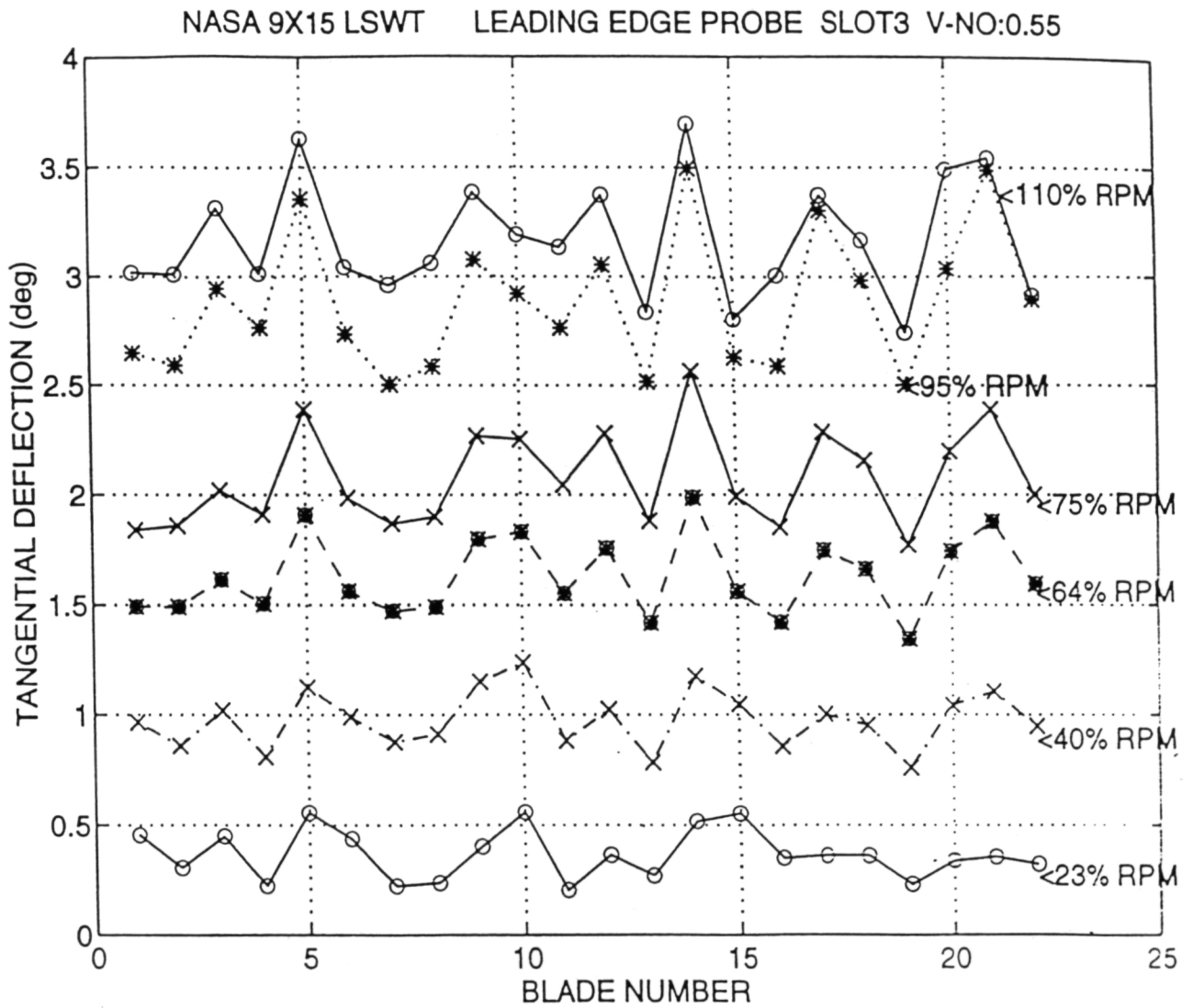


Figure 17: Plot of tangential deflection vs. blade at midchord

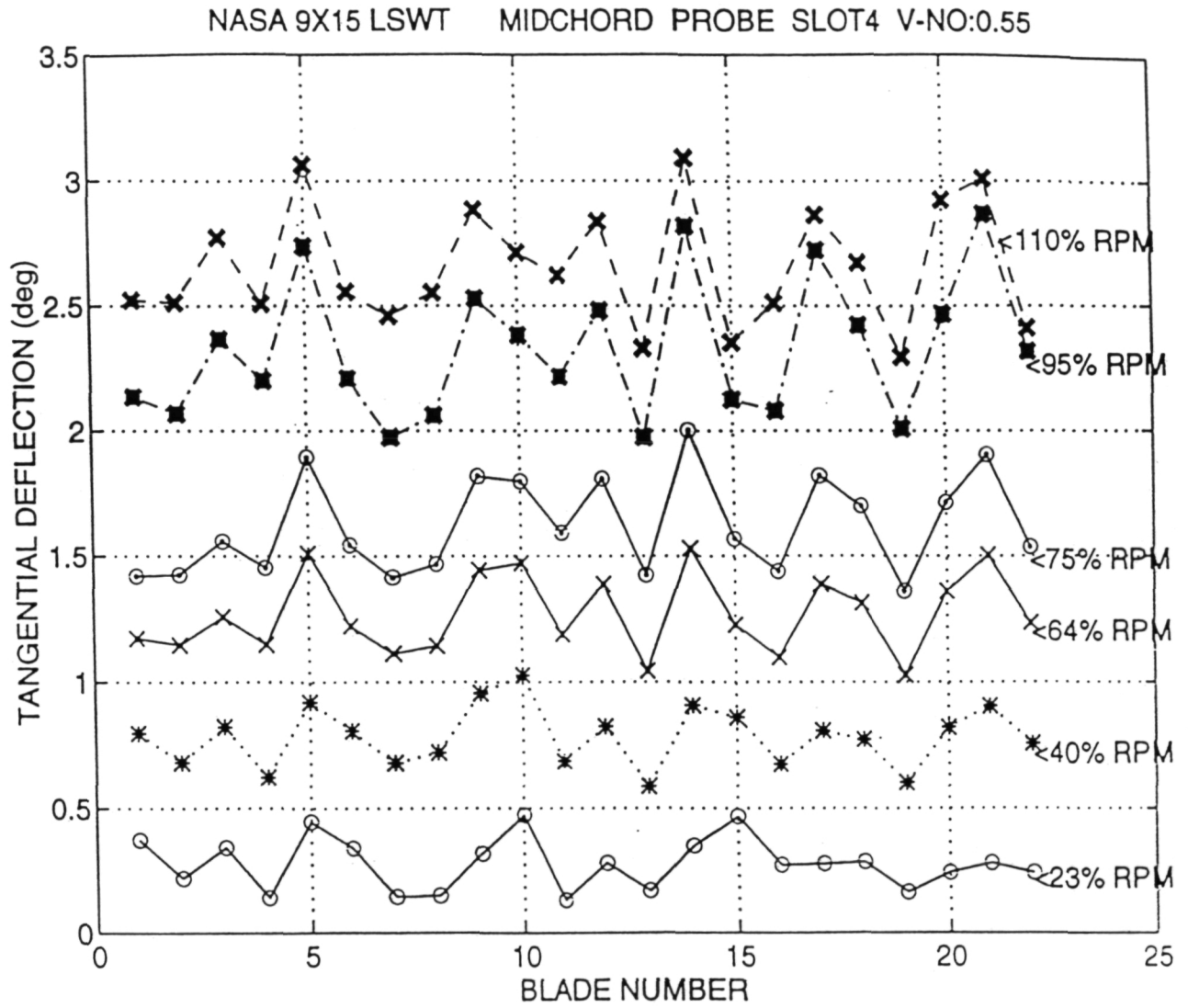
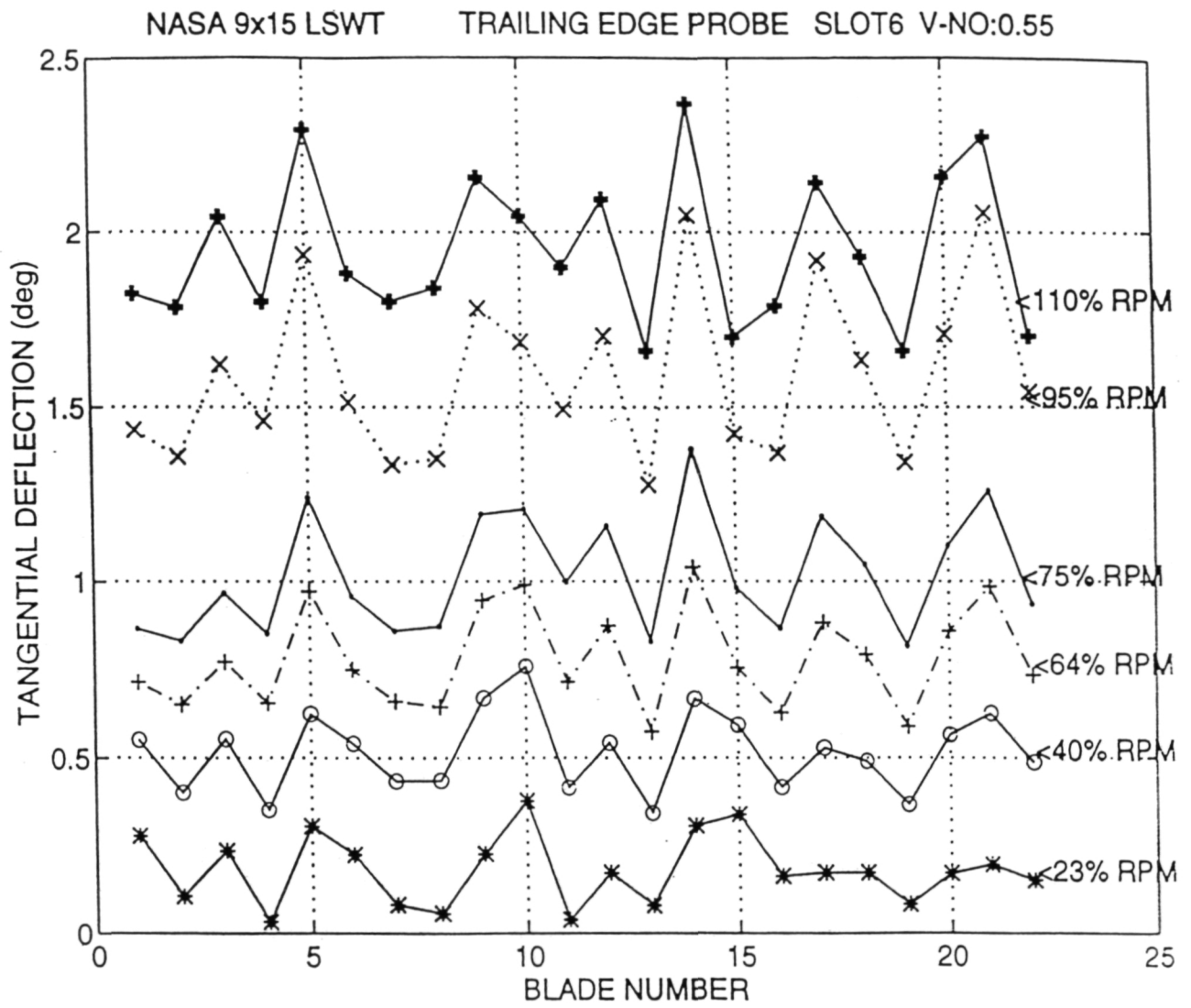


Figure 18: Plot of tangential deflection vs. blade at trailing edge



#### 4. DISCUSSIONS

The fiber optic system described in this report has been successfully used to measure static deflection and fluctuations in blade tip clearance. The system has been thoroughly tested in the laboratory, in a transonic single stage compressor facility and on a scaled aircraft engine in the 9X15 feet subsonic wind tunnel facility at the NASA LeRc. Through the use of integrated fiber optics and avalanche photoreceivers, this system has a very high speed collection efficiency and high gain bandwidth product for the electronic system. The fiber optic probes did not exhibit any degradation in signal quality over 10 hours of continuous use in the aircraft engine environment; this fact is quite remarkable since the probes does not rely on any purging mechanism.

This system opens up new options and opportunities for measurement, condition monitoring, and diagnosis of turbomachinery, particularly combustion turbines with free-standing blades. The sensor electronics can be modified to increase the system bandwidth and to filter out some of the spurious noises. The frequency response is high (greater than 10 MHz.), and fully capable of tracking blade passing signals typical of large combustion turbines or expansion turbines. Low frequency response is also good and static calibration has been demonstrated.

## 5. REFERENCES

1. Kurkov, A.P. & Mehmed, Oral "Optical Measurements of Unducted Fan Flutter", A.S.M.E Journal of Turbomachinery, vol.112, October 1990.
- ✓ 2. W.C. Nieberding and J.L.Pollack, "Optical detection of blade flutter in YF-100 turbofan engine," ASME paper no. 77-GT-66 (NASA TMX-73573)
3. H. Roth, "Vibration measurements on turbomachine rotor blades with optical probes," ASME, Joint Fluids Engineering Gas Turbines Conferences & Products Show, New Orleans, 1980
4. Khan, Romel, "Wavefront Processing Through Integrated fiber optics", PhD dissertation, State University of New York at Stony Brook, 1994.  
Khan, Romel, Dhadwal, H.S., and Suh, K., "Design and Characterization of Coherent Integrated Fiber Optic Imaging Probes," App. Opt., **vol. 33**, pp.5875-5881 (1994)
5. Hohenburg, R., "Detection and Study of Compressor-blade Vibration", Experimental Mechanics, Vol 7, pg 19A-24A, June 1967.
- ✓ 6. Kurkov, A.P. ., " Optical Measurement of Propeller blade Deflections", NASA, Technical Paper 2841, September 1988.
7. Davis, Charles S., "Fiber Optic Sensors: an overviews", SPIE vol 478, Fiber Optic and Laser Sensor II, pg 12-13, 1984.
8. Barranger, J.P & Ford, M.J., "Laser Optical Blade Tip clearance Measurement System", Journal of Engg. for Power, pp 457-460, vol 100, April 1981.
9. Roth, H., "Vibration measurements on turbomachine rotor blades with optical probes", ASME, pp215-224, March 1980.
10. Kurkov, A.P., "Measurements of Self-Excited Rotor-Blade vibrations Using Optical Displacements", Tran. of ASME, pp44-49, vol106, Jan. 1984.
- ✓ 11. Lawrance, C. & Meyr, E.H., "The Use of an Optical Data Acquisition System For Bladed Disk vibration Analysis", NASA T.M. 8689, Dec.1984. *? TM 8689/*
12. Lewis, N.E., Miller, M.B., and Lewis, W.H., "Fiber Optic Sensors Utilizing Surface Reflections", SPIE vol 478, Fiber optic and Laser Sensors II, pg 39-42, 1984.
13. Debney, B.T., and Carter, A.C., " Optical Fibers Sensors: Principle and Components", pg 107-147, vol 1, 1988, Artech House., Inc., Boston and London.
14. Linear Application Databook, National Semiconductor, 1986.
15. Motorola Linear/Interface Devices Data Book, 1989.
16. Logic Data Book, vol II, National Semiconductor, 1984.
17. Krohn, David A., " Intensity modulated Fiber Optic Sensors", SPIE vol. 718, Fiber Optic and Laser Sensors IV , pg 2-7, 1986.
18. Culshaw, B., "Optical Fibers Sensors: Principle and Components", pg 9-23, vol 1, , 1988, Artech House., Inc., Boston and London.
19. Conley, M.P., Zarobila, C.J., Freal, J.B., " Reflection Type Fiber optic Sensor", SPIE vol 718, Fiber optic and Laser Sensors IV, pg 237, 1986.

APPENDICES

# Design and characterization of coherent integrated fiber-optic imaging probes

Romel R. Khan, Harbans S. Dhadwal, and Kwang Suh

An integrated fiber-optic probe comprising a short length of multimode fiber that is fusion spliced to a monomode optical fiber has been fabricated for imaging and nonimaging applications. The fiber probe, typically 250  $\mu\text{m}$  in diameter, can deliver a focused Gaussian spot approximately 25  $\mu\text{m}$  in diameter at a distance of approximately 500  $\mu\text{m}$  from the tip. Two off-the-shelf graded-index multimode fibers have been used in the fabrication of imaging and nonimaging probes. These integrated probes have considerably improved the spatial resolution of backscatter lensless fiber probes being utilized in the dynamic light-scattering characterization of colloidal suspension.

## 1. Introduction

Here we report the design and characterization of integrated fiber-optic probes, comprising a monomode optical fiber that is fusion spliced to a short length of a graded-index multimode fiber, for delivery of either a collimated beam or a focused spot to a remote location. An experimental result of the application of a graded-index multimode-fiber lens (GFL) in a laser light backscattering fiber-optic probe (BFOP), which was described in Dhadwal *et al.*,<sup>1</sup> is also presented. So far these compact BFOP's have not used any lens. The use of a lens to deliver a focused spot and another lens to receive light from a small scattering volume will enhance the resolution of the BFOP without increasing its size and without degrading the self-beating efficiency<sup>2</sup> of the laser light scattering system.

There have been several earlier studies on the uses of the GFL. Dhadwal *et al.*<sup>3</sup> used the integrated GFL probes as coherent receivers in dynamic light scattering. Emkey and Jack<sup>4</sup> evaluated them in connection with the development of miniaturized low-loss fiber-optic connectors. Watson<sup>5</sup> used the GFL's to make a linear array of microlenses. Mathyssek *et al.*<sup>6</sup> used them in laser diode to single-mode fiber coupling. Liou<sup>7</sup> used a GFL as an external cavity for an InGaAsP buried-heterostructure laser.

Advantages of GFL's include size compatibility with monomode optical fibers and an overall reduction in size by a factor of 10 over Selfoc<sup>8</sup> graded-index lenses manufactured by Nippon Sheet Glass.<sup>8</sup> We obtain variation in the image distance and magnification by controlling the length,  $L$ , of the GFL. The object distance in this paper is fixed to zero because the monomode fiber is fused to the lens, resulting in a rugged and compact probe that does not require alignment of the lens.

We note that a multimode graded-index optical fiber with a quadratic refractive-index profile [see Eq. (1)] has focusing properties similar to those of spherical lenses and Selfoc lenses. Many commercially available fibers, such as those made by modified chemical vapor deposition<sup>9</sup> methods, have a large central index depression. In general, a large deviation from the quadratic index profile may result in a great degradation of the imaging quality of a GFL. Two multimode fibers, Corning 50/125- $\mu\text{m}$  fiber (or Newport Model MSD) and Corning 100/140- $\mu\text{m}$  fiber (or Newport Model MLD), have been considered here. In Section 2 GFL parameters such as beam waist and image distance are found through the use of a ray-matrix analysis for a Gaussian wave. In Section 3 experimental results are presented.

## 2. Theoretical Background

Figure 1 shows a schematic of a generic integrated coherent fiber-optic probe. The refractive-index profile of the fibers considered here is approximated to be in the form

$$n^2(r) = n_0^2[1 - (g_0 r)^2], \quad (1)$$

The authors are with the Department of Electrical Engineering, State University of New York at Stony Brook, Stony Brook, New York 11794-2350.

Received 3 June 1993; revised manuscript received 7 January 1994.

0003-6935/94/255875-07\$06.00/0.

© 1994 Optical Society of America.

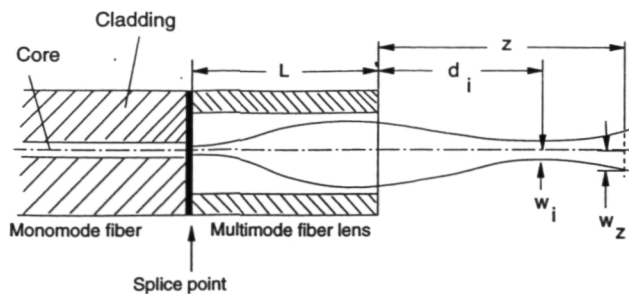


Fig. 1. Schematic of an integrated fiber-optic probe.

where  $r$  is the radial distance from the optical axis,  $n_0$  is the on-axis refractive index, and  $g_0$  is the quadratic index constant. Neglecting aberration effects, we see that the pitch,  $P$ , of the fiber is given by<sup>9</sup>

$$P \approx \frac{2\pi}{g_0}. \quad (2)$$

The optical field distribution radiating from the tip of a monomode fiber can be approximated by a Gaussian profile<sup>10</sup> having a beam waist (or beam radius)  $w_0$ . In our study we used a monomode fiber (Newport Model FSV) with a core radius of  $2 \mu\text{m}$  whose mode field radius (or  $w_0$ ) is quoted to be  $2.3 \mu\text{m}$  by the manufacturer. Following the ray-matrix analysis given by Gomez-Reino and others,<sup>11,12</sup> we see that the complex input ray position and slope for a Gaussian wave are given by  $r_1 = w_0$  and  $\dot{r}_1 = j\lambda/(\pi n_0 w_0)$ , respectively. Here  $\lambda$  is the wavelength of light. The complex input is related to the complex output position  $r_2$  and slope  $\dot{r}_2$ , at a distance  $z$  from the tip of the GFL (see Fig. 1), by

$$\begin{bmatrix} r_2 \\ \dot{r}_2 \end{bmatrix} = \begin{bmatrix} A & B \\ C & D \end{bmatrix} \begin{bmatrix} r_1 \\ \dot{r}_1 \end{bmatrix}, \quad (3)$$

where

$$\begin{bmatrix} A & B \\ C & D \end{bmatrix} = M_{43} M_{32} M_{21},$$

$$M_{21} = \begin{bmatrix} \cos(g_0 L) & \sin(g_0 L)/g_0 \\ -g_0 \sin(g_0 L) & \cos(g_0 L) \end{bmatrix},$$

is the transmission matrix within the GFL where  $L$  is the length of the GFL. Note that

$$M_{32} = \begin{bmatrix} 1 & 0 \\ 0 & n_0 \end{bmatrix}$$

is the refraction matrix from a GFL to air, and

$$M_{43} = \begin{bmatrix} 1 & z \\ 0 & 1 \end{bmatrix}$$

is the transmission matrix in air.

The beam waist,  $w_z$ , is given by the absolute value of  $r_2$ ,

$$w_z^2 = w_0^2 \left\{ [\cos(2\pi\eta) - n_0 z g_0 \sin(2\pi\eta)]^2 + a^2 \left[ \frac{\sin(2\pi\eta)}{g_0} + n_0 z \cos(2\pi\eta) \right]^2 \right\}, \quad (4)$$

where the fractional pitch  $\eta = L/P$  is in the range 0–1.0 and  $a = \lambda/(\pi n_0 w_0^2)$ .

Minimizing  $w_z$  with respect to  $z$  gives image distance  $d_i$  and image magnification  $m_g$  (Ref. 13):

$$d_i = \frac{\sin(4\pi\eta)(g_0^2 - a^2)}{2n_0 g_0 [g_0^2 \sin^2(2\pi\eta) + a^2 \cos^2(2\pi\eta)]}, \quad (5)$$

$$m_g = \frac{w_i}{w_0} = \frac{1}{\left[ \left[ \frac{g_0 \sin(2\pi\eta)}{a} \right]^2 + \cos^2(2\pi\eta) \right]^{1/2}}, \quad (6)$$

The divergence angle of the output Gaussian beam from the image point is inversely proportional to image beam waist  $w_i$  and is given by

$$\Delta\theta = \frac{\lambda}{\pi w_i} = \frac{\lambda}{\pi w_0 m_g}. \quad (7)$$

Figures 2 and 3 show plots of image distance  $d_i$  and magnification  $m_g$  as a function of  $\eta$  for MLD and MSD fibers, respectively, whose characteristic parameters are shown in Table 1. All results are at a wavelength of  $0.633 \mu\text{m}$ . From these figures we can see that for  $\eta = 0.25$  the image is formed on the back surface of the GFL, with the highest magnification and the lowest divergence; such a GFL is best for producing a collimated output. In general, one can use Figs. 2 and 3 for fabricating an integrated fiber probe with a desired imaging condition based on the image distance, magnification, and divergence requirements.

Figure 4 shows a plot of  $w_z$  as a function of  $z$  for  $0.25P$  MSD GFL (dashed curve) and  $0.25P$  MLD GFL (solid curve). We note that divergence of the MLD GFL is lower than that of the MSD GFL. For  $z < 4$  mm, a beam waist of less than  $60 \mu\text{m}$  can be obtained.

We can find maximum image distance  $d_{im}$  at  $\eta = \eta_m$  analytically from Eq. (5) by maximizing  $d_i$  with respect to  $\eta$ ,

$$\eta_m = \frac{1}{2\pi} \tan^{-1} \left( -\frac{a}{g_0} \right), \quad (8)$$

evaluated in second quadrant, and

$$d_{im} = \frac{a^2 - g_0^2}{2n_0 a g_0^2}. \quad (9)$$

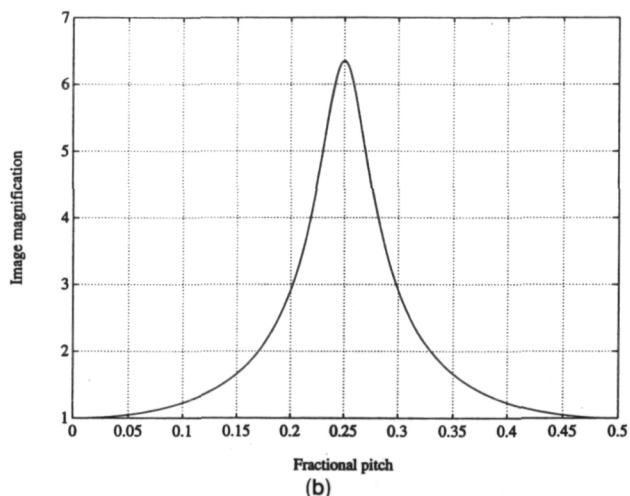
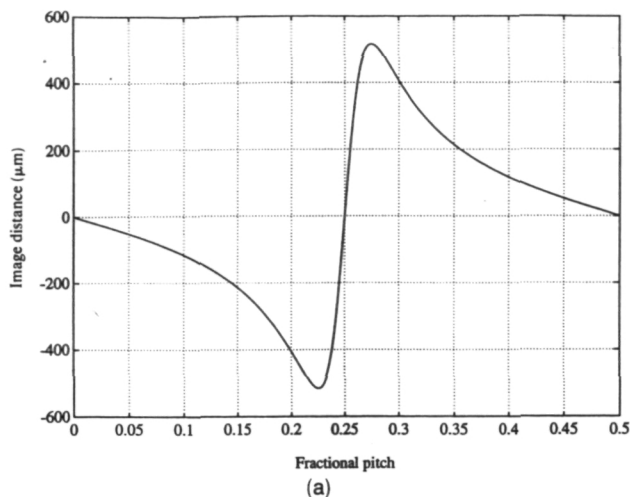


Fig. 2. Theoretical plots for the imaging properties of MLD GFL at  $\lambda = 0.633 \mu\text{m}$ : (a) image distance  $d_i$  (in micrometers) versus fractional pitch  $\eta$  [Eq. (5)], (b) image magnification  $m$  versus fractional pitch  $\eta$  [Eq. (6)].

For MSD GFL,  $\eta_m = 0.284$  and  $d_{im} = 274 \mu\text{m}$ , whereas for MLD GFL,  $\eta_m = 0.275$  and  $d_{im} = 516 \mu\text{m}$ . Note that one could use Eq. (9) to specify optimum values of  $g_0$  and  $n_0$ , hence the index profile [Eq. (1)], to achieve desired values of  $d_{im}$ . For example, to achieve a maximum image distance of 5 mm at  $\lambda = 0.633 \mu\text{m}$  with  $n_0 = 1.47$ , one should fabricate a GFL with  $g_0 = 1.33 \text{ mm}^{-1}$ . The theoretical prediction for the intensity distribution at distance  $z$  from the tip of the GFL is given by<sup>13</sup>

$$I_z = I_0 \exp\left(-\frac{2r^2}{w_z^2}\right), \quad (10)$$

where  $w_z$  is given by Eq. (4).

As we mentioned earlier, the theory presented above is derived through the use of ray matrices. For GFL's, which have a diameter comparable with the wavelength of light, diffraction effects must be taken into account. We define the rms relative error

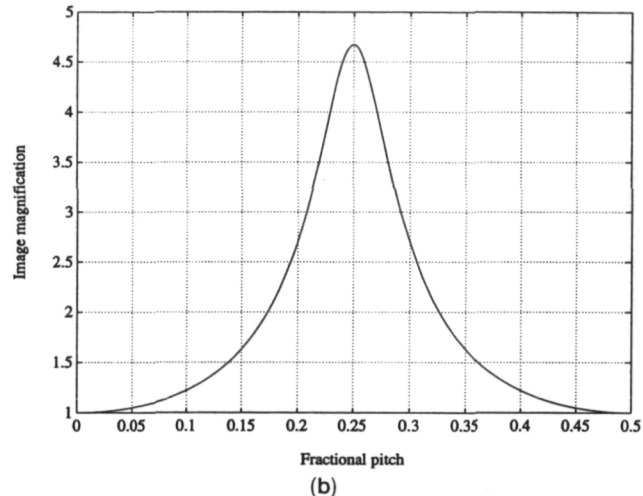
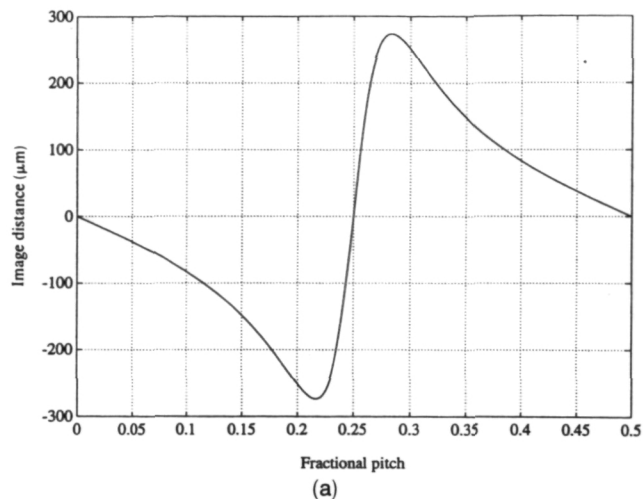


Fig. 3. Theoretical plots for the imaging properties of MSD GFL at  $\lambda = 0.633 \mu\text{m}$ : (a) image distance  $d_i$  (in micrometers) versus fractional pitch  $\eta$  [Eq. (5)], (b) image magnification  $m$  versus fractional pitch  $\eta$  [Eq. (6)].

caused by diffraction as

$$\epsilon = \left[ \frac{\int_0^{w_2} (I_d - I_{nd})^2 d\rho}{\int_0^{w_2} I_{nd}^2 d\rho} \right]^{1/2}, \quad (11)$$

where  $w_2$  is the beam waist on the output surface of the lens. Here  $I_{nd}$  and  $I_d$  are the intensity distributions assuming no diffraction and diffraction, respec-

Table 1. Characteristic Parameters of MSD and MLD Fibers

Fiber Type	$n_0$	$g_0$ ( $\text{mm}^{-1}$ )	Diameter $d$ (mm)	On-axis N.A.
MSD	1.4713	5.54	0.050	0.2
MLD	1.4815	4.05	0.1	0.3

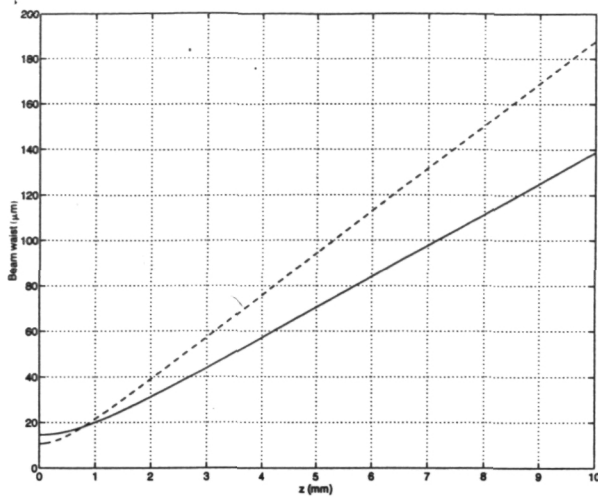


Fig. 4. Theoretical plots of beam waist  $w_z$  (in micrometers) versus axial distance  $z$  for a  $0.25P$  lens, through the use of Eq. (4), at  $\lambda = 0.633 \mu\text{m}$ . The solid curve represents MLD GFL and the dashed curve represents MSD GFL.

tively. We have derived  $I_d$  by using the diffraction analysis given by Liñares and Gómez-Reino.<sup>14,15</sup> Using Eq. (11), we found that for MSD GFL,  $\epsilon < 0.7\%$  and for MLD GFL,  $\epsilon < 0.02\%$  for  $0 < \eta \leq 0.5$  at  $\lambda = 0.633 \mu\text{m}$ ; therefore, for these two GFL's diffraction effects are negligible and the ray theory presented should suffice.

### 3. Experimental Procedure and Results

#### A. Output Field Characterization

Details of the fabrication process for an integrated fiber probe are described by Dhadwal *et al.*<sup>3</sup> and are not repeated here. Figure 5 shows a schematic of the system for characterizing a GFL. A He-Ne laser (Melles Griot Model GLD5261) was launched into the free end of the monomode fiber by means of a  $20\times$  microscope objective. We used a fiber coupled to a power meter (Newport Model 835) to record the transverse intensity distribution at various  $z$  positions.

Figures 6–8 show the theoretical (solid curve) and experimental (circles) intensity versus the transverse distance relationship for MLD  $0.225P$ , MLD  $0.255P$ , and MSD  $0.234P$  GFL's, respectively. The  $\times$ 's in these figures show the experimental readings with an unlensed monomode fiber, confirming that the lensed fibers are producing narrower beams. The dashed curves are the expected output from a  $0.25P$  GFL.

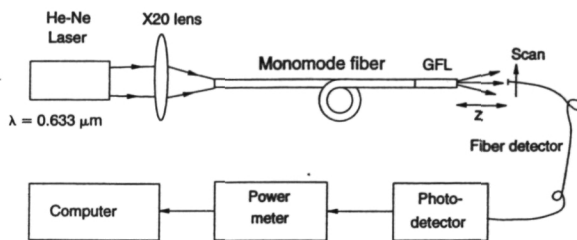


Fig. 5. Schematic of the system for characterizing a GFL.

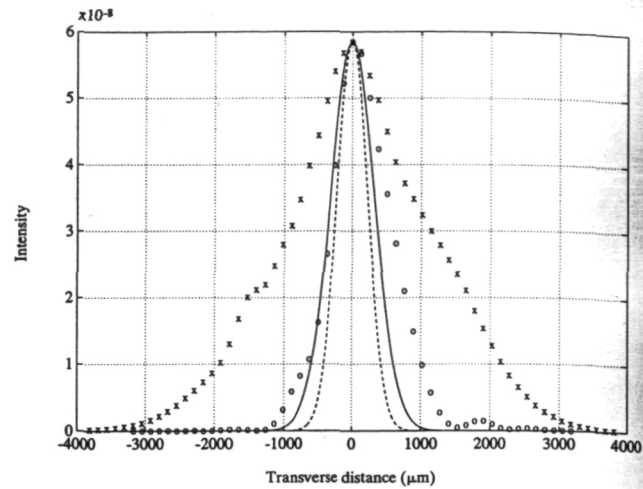


Fig. 6. Characterization of the intensity distribution for MLD GFL with  $0.225P$  length: circles, measured data points at  $z = 33$  mm; solid curve, expected distribution through the use of Eq. (10); dashed curve, expected distribution for a  $0.25P$  lens;  $\times$ 's, measured data from an unlensed monomode fiber at  $z = 33$  mm.

The dashed and solid curves of Fig. 7 are almost superimposed because the length of MLD  $0.255P$  GFL is very close to  $0.25P$ . All intensity distributions shown, except those of Fig. 8, were taken at  $z = 33$  mm. Distributions in Figs. 8(a) and 8(b) were taken at  $z = 7.6$  and  $25.4$  mm, respectively. From Fig. 8 it is clear that the spot size of the unlensed fiber is growing at a greater rate, implying a larger divergence than that of lensed fibers. Another point to note is that the match between theory and experiment remains consistent for different distances.

MLD GFL's seem to show a greater aberration or excitation of higher-order modes than MSD GFL's, and the correlation between experiment and theory is less for the former GFL's than for the latter. The reason for this is that MLD fibers have a greater central index depression than MSD fibers (MSD fibers approximate a quadratic profile more closely than MLD fibers).<sup>16</sup>

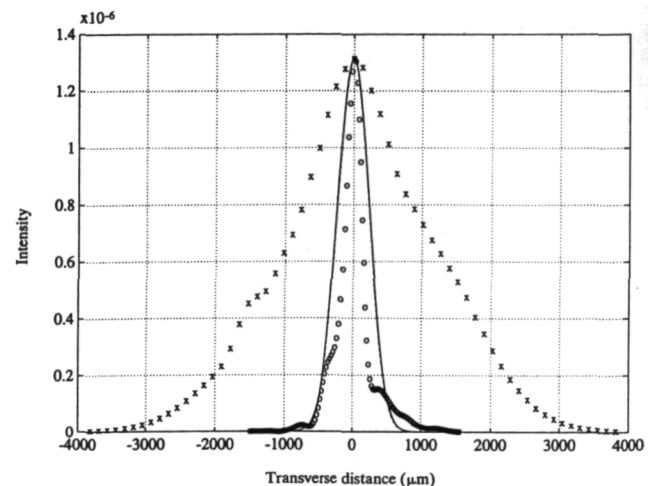


Fig. 7. Characterization of the intensity distribution for MLD GFL with  $0.255P$  length. Symbols are the same as in Fig. 6.

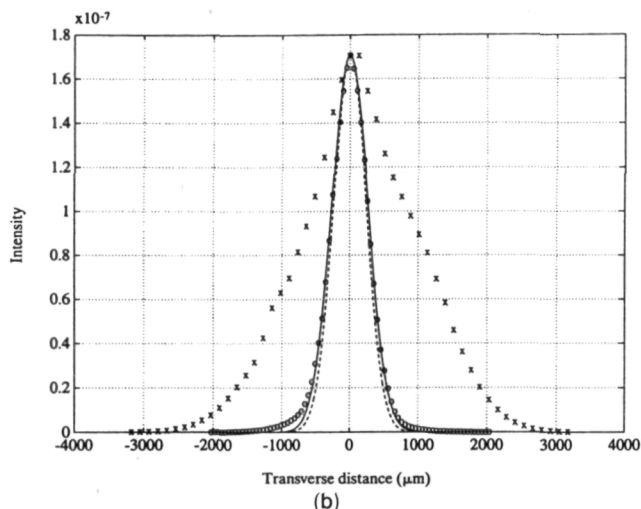
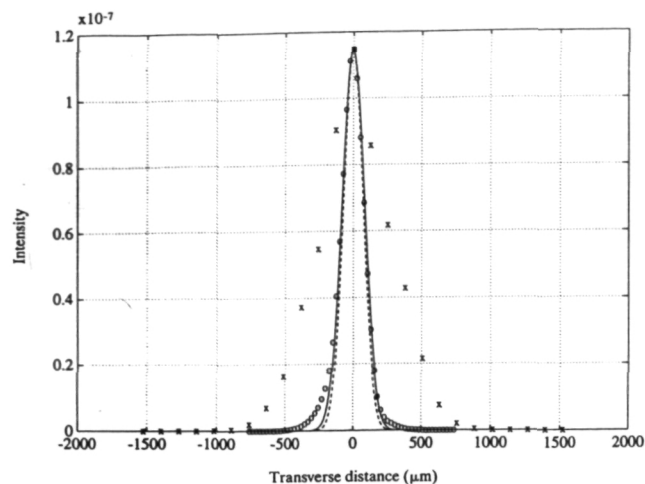


Fig. 8. Characterization of the intensity distribution for MSD GFL with 0.234P length: (a)  $z = 7.6$  mm, (b)  $z = 25.4$  mm. Symbols are the same as in Fig. 6.

#### B. Application of GFL in Dynamic Laser Light BFOP

In the past 5 years considerable advances have been made in the utilization of dynamic light scattering techniques for the characterization of the size distribution of submicroscopic particles contained in oddly shaped containers, which are positioned in remote locations.<sup>1,3,17-20</sup> This has been made possible through the use of coherent backscatter probes described by Dhadwal *et al.*<sup>1</sup> It suffices for us to note here that the BFOP achieves the high self-beating efficiency of conventional laboratory-based systems, but it lacks the spatial resolution that may be necessary in certain applications. This compromise was necessary so the required miniaturization could be retained without the use of additional bulk optics such as lenses, which at best would increase the overall diameter of the BFOP tenfold. This paper demonstrates that through the use of integrated fiber optics, one can considerably enhance the spatial resolution of the BFOP without increasing the size of the BFOP.

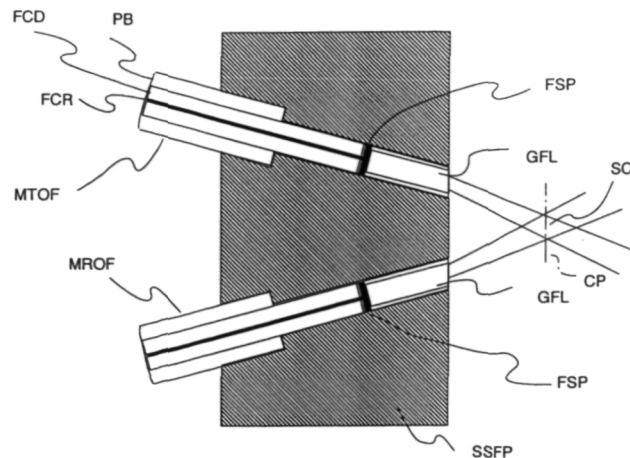


Fig. 9. Lensed backscatter fiber-optic probe: FCD, fiber cladding; FCR, fiber core; PB, polymer buffer; FSP, fusion splice point; MTOF, monomode transmitting fiber; MROF, monomode receiving fiber; SC, scattering region; CP, crossover plane; SSFP, stainless steel faceplate.

Readers who are interested in learning about the theory and practice of laser light scattering are referred to Chu's textbook.<sup>2</sup> We fabricated two lensed fibers and mounted them in the same housing (ferrule), see Fig. 9, for delivering light and receiving scattered light from particles executing Brownian motion. The backscattering angle for the lensed probe was measured to be  $150^\circ$  in water. We used MSD fiber as the GFL because its cladding diameter ( $125 \mu\text{m}$ ) matched that of the FSV monomode fiber, and because the field output of MSD GFL is cleaner than that of MLD GFL, as we mentioned in Subsection 3.A. For best performance, both MSD GFL's should be  $0.25P$  (or  $283 \mu\text{m}$ ) long. Our BFOP has MSD GFL's that are  $\sim 200 \mu\text{m}$  long. Figure 10 shows the output intensity from a lensed fiber used in

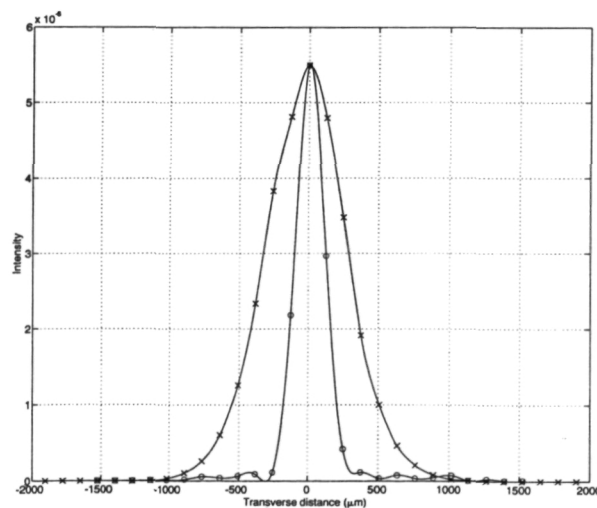


Fig. 10. Output intensity versus transverse distance (in micrometers) for lensed fiber used in a lensed BFOP (circles) with a  $205\text{-}\mu\text{m}$  waist and for unlensed fiber used in an unlensed BFOP ( $\times$ 's) with a  $570\text{-}\mu\text{m}$  waist at the crossover region. Solid curves are splines through the  $\times$ 's and circles.

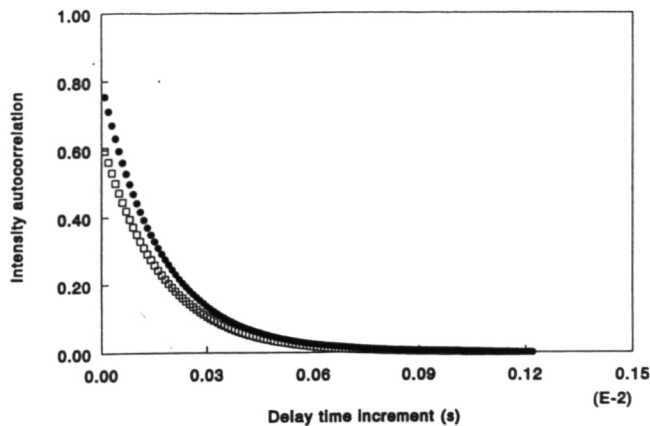


Fig. 11. Normalized intensity autocorrelations obtained from an aqueous suspension of 85-nm polystyrene latex spheres, through the use of the lensed BFOP (circles) and the unlensed BFOP (squares).

the lensed BFOP (circles) and the output from an unlensed fiber used in an equivalent unlensed BFOP ( $\times$ 's) at the crossover plane. It is obvious that the lensed BFOP device has the potential of having a higher spatial resolution because its beam width is narrower than the unlensed BFOP.

For particle sizing analysis, we used an aqueous suspension of polystyrene latex spheres with a nominal average diameter of 85 nm. The BFOP's were used with a compact laser diode module that was described by Dhadwal *et al.*<sup>20</sup> A laser diode (Toshiba Model 9215) was used for delivering light, and a photomultiplier tube (Hamamatsu Model HC-120) was used for photon detection. Figure 11 shows an intensity-intensity autocorrelation obtained for a lensed BFOP (circles) and an unlensed BFOP (squares). We used a digital correlator (Brookhaven Instruments Model BI9000) to obtain the data. Figure 12 shows the corresponding size distribution obtained by the use of a nonnegative least-squares inversion procedure. Both the lensed and the un-

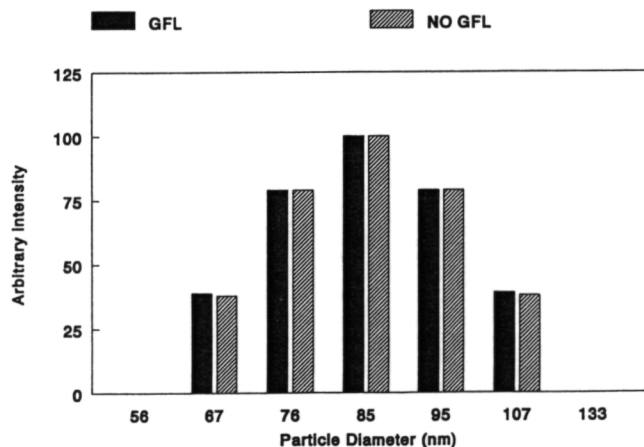


Fig. 12. Size distribution obtained from the inversion of the two correlation data in Fig. 11 through the use of a nonnegative least-squares data-inversion technique. Inverted data are identical.

lensed BFOP's give an identical distribution of particle size, which is consistent with our expectation. The average signal-to-noise ratio or the self-beating efficiency for the lensed BFOP was close to (slightly higher than) the unlensed BFOP over many runs. However, the significant increase in spatial resolution, by a factor of 2, makes the lensed BFOP indispensable in the study of systems in which the scattering may be confined to a small region, e.g., characterization of protein crystallins in a human eye lens.<sup>18</sup>

#### 4. Summary

We have described the design of integrated fiber-optic imaging probes. For the GFL's considered here, a maximum image distance of  $\sim 500 \mu\text{m}$  can be achieved with a magnification of  $\sim 5$ . For a detection distance of less than 4 mm, a beam waist of less than  $60 \mu\text{m}$  can be obtained. Output intensities from the GFL's have been in close agreement with theoretical expectations. An application of GFL's in laser light back-scattering fiber-optic probes is also presented. The integrated fiber-optic probes described here can be customized for a variety of diverse applications. Our results were obtained through the use of two commercially available graded-index multimode optical fibers. However, other optimizations may be achieved through the fabrication of multimode fibers with specified index profiles.

We thank W. Emkey of AT&T Bell Laboratories at Breinigsville for allowing access to the fusion splicer and C. Jack for his assistance and patience in using the splicer. We acknowledge continuous support from NASA under contracts NCC3-241 and NAG3-1526.

#### References and Notes

1. H. S. Dhadwal, R. R. Ansari, and W. V. Meyer, "A fiber optic probe for particle sizing in concentrated systems," *Rev. Sci. Instrum.* **63**, 2963-2968 (1993).
2. B. Chu, *Laser Light Scattering* (Academic, New York, 1991).
3. H. S. Dhadwal, R. R. Khan, and K. Suh, "An integrated fiber optic probe for dynamic light scattering," *Appl. Opt.* **32**, 3901-3904 (1993).
4. W. L. Emkey and C. A. Jack, "Analysis and evaluation of graded index fiber lenses," *J. Lightwave Technol.* **LT-5**, 1156-1164 (1987).
5. H. Watson, "A linear array of twelve graded-index lenses butted coaxially against single mode fibers using silicon V-groove technology," in *Optical Fiber Communication*, Vol. 4 of OSA 1991 Technical Digest Series (Optical Society of America, Washington, D.C., 1991), p. 149.
6. K. Mathyssek, R. Keil, and E. Clement, "New coupling arrangement between laser diode and single mode fiber with high coupling efficiency and particularly low feedback effect," in *Optical Communication, ECOC '84*, H. Haupt, ed. (North-Holland, New York, 1984), pp. 186-187.
7. K. Y. Liou, "Single-longitudinal-mode operation of injection laser coupled to a grating external cavity," *Electron. Lett.* **19**, 750-751 (1983).
8. Sefloc is a trademark of Nippon Sheet Glass Company, Osaka, Japan.
9. T. Okoshi, *Optical Fibers* (Academic, New York, 1982), Chaps. 2 and 3.

10. D. Marcuse, "Gaussian approximation of the fundamental modes of graded-index fibers," *J. Opt. Soc. Am.* **68**, 103-109 (1978).
11. E. Acosta, J. Flores, C. Gómez-Reino, and J. Liñares, "Gradient index lens law for Gaussian illumination: image and focal shifts," *Opt. Eng.* **28**, 1168-1172 (1989).
12. C. Gómez-Reino and J. Liñares, "Paraxial Fourier transforming and imaging properties of a GRIN lens with revolution symmetry: GRIN lens law," *Appl. Opt.* **25**, 3418-3424 (1986).
13. H. S. Dhadwal, R. R. Khan, and K. Suh, "Integrated coherent imaging fiber optics," presented at the Tenth Topical Meeting on Gradient-Index Optical Systems, Santiago de Compostela, Galicia, Spain, 1992.
14. J. Liñares and C. Gómez-Reino, "Diffraction-limited coupling efficiency between SMF connected by GRIN fiber lenses," *J. Mod. Opt.* **38**, 597-604 (1991).
15. J. Liñares and C. Gómez-Reino, "Pupil effect in a GRIN lens with Gaussian illumination," *J. Mod. Opt.* **38**, 481-494 (1991).
16. See Corning Product information sheets for 50/125 and 100/140 fibers (issued July 1990).
17. R. R. Ansari, H. S. Dhadwal, M. Cheung, and W. Meyer, "Microemulsion characterization using a fiber optic probe," *Appl. Opt.* **32**, 3822-3827 (1993).
18. H. S. Dhadwal, R. R. Ansari, and M. A. Dellavecchia, "A coherent fiber optic sensor for early detection of cataractogenesis in a human eye lens," *Opt. Eng.* **32**, 223-238 (1993).
19. H. S. Dhadwal, W. Wilson, R. R. Ansari, and W. Meyer, "Dynamic light scattering studies of BSA and Lysozyme using a backscatter fiber optic system," in *Static and Dynamic Scattering in Medicine and Biology*, R. J. Nossal, R. Pecora, and A. V. Priezzhev, eds., *Proc. Soc. Photo-Opt. Instrum. Eng.* **1884**, 16-24 (1993).
20. H. S. Dhadwal, K. Suh, and R. R. Khan, "Compact backscatter fiber optic systems for submicroscopic particle sizing," submitted to *J. Partic. Process. Sci. Technol.*

ORIGINAL PAGE IS  
OF POOR QUALITY